



Alexandria University
Alexandria Engineering Journal

www.elsevier.com/locate/aej
www.sciencedirect.com



ORIGINAL ARTICLE

Parametric analysis of a 4-stroke GDI engine using CFD

S. Krishna Addepalli, Mallikarjuna J.M. *

Internal Combustion Engine Laboratory, Department of Mechanical Engineering, Indian Institute Technology Madras, Chennai 600036, India

Received 11 August 2016; revised 3 October 2016; accepted 25 October 2016
 Available online 12 November 2016

KEYWORDS

GDI engine;
 Engine parameters;
 CFD;
 Performance characteristics

Abstract The present study focuses on the evaluation of the effect of engine parameters on the characteristics of a GDI engine by CFD analysis. The analysis was carried out at three engine speeds (2000, 3000, and 4000 rev/min), at three compression ratios (10, 11, and 12) and at three fuel injection pressures (200, 300, and 400 bar). The overall equivalence ratio of the in-cylinder mixture was maintained at 0.75 in all the above cases. Finally, it is observed that, the turbulent kinetic energy and tumble ratio were more sensitive to the engine speed than to other parameters. The fuel injection pressure was found to play a vital role in obtaining combustible mixture near the spark plug at the time of spark. In addition, a low heat release rate occurred at the engine speed of 4000 rev/min compression ratio of 10 and fuel injection pressure of 200 bar.

© 2016 Faculty of Engineering, Alexandria University. Production and hosting by Elsevier B.V. This is an open access article under the CC BY-NC-ND license (<http://creativecommons.org/licenses/by-nc-nd/4.0/>).

1. Introduction

Today, carburetors are replaced by electronic fuel injection systems in spark ignition engines, where mixture strength can be controlled easily, in order to control emissions [1,2]. However, fuel economy and emissions with these systems may not improve significantly. Therefore, today GDI technology is becoming very popular [3]. In GDI engines, fuel injection happens directly into the engine cylinder very precisely, which in turn helps improve both performance and emission characteristics [4]. The major advantage is that it can be operated with a lean stratified mode over a wide range of operating con-

ditions, thus reducing the fuel consumption. There are many factors that affect the performance and emission characteristics of GDI engines [5].

Suresh Kumar et al. [6] studied the effect of piston crown shape on in-cylinder flow characteristics of a two-valve GDI engine by using CFD analysis. They concluded that the piston with a bowl preserved the tumble motion inside the engine cylinder for a longer time than the flat piston, and thus reduced cycle-by-cycle variations. Oh and Bae [7] investigated the effect of fuel injection timing on spray and combustion characteristics in a spray-guided direct injection SI (DISI) engine under a lean stratified operation. They analyzed combustion and fuel spray characteristics using PLIF technique. They found that non-luminous and luminous flames were dominant with advanced and retarded fuel injection timings respectively. Also, NO_x emissions decreased and IMEP increased with retarded injection timing. Baecker et al. [8] performed investigations on a spray-guided GDI engine operated at a stratified

* Corresponding author.

E-mail addresses: krsna100@gmail.com (S.K. Addepalli), jmallik@iitm.ac.in (J.M. Mallikarjuna).

Peer review under responsibility of Faculty of Engineering, Alexandria University.

<http://dx.doi.org/10.1016/j.aej.2016.10.007>

1110-0168 © 2016 Faculty of Engineering, Alexandria University. Production and hosting by Elsevier B.V.

This is an open access article under the CC BY-NC-ND license (<http://creativecommons.org/licenses/by-nc-nd/4.0/>).

Abbreviations

AMR	adaptive mesh refinement	PISO	pressure implicit with splitting of operators
BDC	bottom dead center	PLIEF	planar laser induced exciplex fluorescence
CAD	crank angle degree	PLIF	planar laser induced fluorescence
CAI	controlled auto ignition	SI	spark ignition
CFD	computational fluid dynamics	SMD	Sauter mean diameter
CO	carbon monoxide	SR	swirl ratio
CR	compression ratio	TDC	top dead center
DMF	2,5-dimethylfuran	TKE	turbulent kinetic energy
GDI	gasoline direct injection	TR	tumble ratio
HC	hydrocarbon	IVO	inlet valve opening
IMEP	indicated mean effective pressure	IVC	inlet valve closing
kh-rt	Kelvin Helmholtz-Rayleigh Taylor	EVO	exhaust valve opening
NOx	nitric oxides	EVC	exhaust valve closing
PDPA	phase doppler particle analysis		

mode with single and double fuel injection strategies. Experimental and numerical investigations were carried out using a combustion chamber endoscopy and CFD analysis respectively to evaluate emission and performance characteristics of the engine. They found that the double injection strategy offered a clear advantage in terms of fuel consumption especially at higher loads. Also, their predicted fuel spray penetration and evaporation rate matched well with the experimental data. Stan et al. [9] simulated mixture formation and combustion processes of a four-stroke four-valve single-cylinder GDI engine at various engine speeds and loads, in order to optimize injector opening pressure and duration, and injection system configuration. Also, they analyzed non-homogeneity of mixture and the influence of additional spark on the combustion. They found that the existing simulation codes were not adequate enough to analyze hydrodynamic processes of fuel injection systems, internal mixture formation and combustion. However, they found that the simulation could give more insight into the problem than the experiments. Lee and Park [10] studied the internal structure of a liquid jet from a multi-hole GDI injector using PDPA system. Also, they studied fuel spray breakup process under the injection pressure of about 30 MPa, in order to analyze atomization process. They reported that the SMD of fuel droplets decreased linearly, when the fuel injection pressure was increased from 5 to 10 MPa and from 10 to 20 MPa. However, at the fuel injection pressure beyond 20 MPa, there were no significant changes in the SMD of droplets. Sementa et al. [11] studied spray and combustion evolution with gasoline and ethanol as fuels, in a high performance GDI engine using UV-visible digital imaging. They found that the gasoline spray was more sensitive to air motion and in-cylinder pressure than those of ethanol, for all the conditions considered. Zheng et al. [12] used the AVL-FIRE in order to study mixture preparation and combustion in a wall guided GDI engine using four piston shapes. They concluded that, a flat-top piston with a pit was beneficial to maintain in-cylinder turbulence intensity and promote fuel evaporation. Costa et al. [13] analyzed mixture formation and combustion process in a lean burn GDI engine using experimental (UV-visible digital imaging) and numerical (AVL-FIRE) techniques. They concluded that piston head

geometry played an important role in the mixture formation in the wall guided GDI engines.

From the above discussion, it is observed that many researchers have focused on various aspects of GDI engines. However, a comprehensive understanding of the effect of engine parameters on the performance and emission characteristics of a GDI engine has not been dealt with. Therefore, the aim of this paper is to evaluate the effect of various engine parameters on the performance and emission characteristics of a GDI engine. This analysis will be helpful to optimize the GDI engine parameters for efficient operation.

2. Geometrical details

In this study, a single-cylinder four-stroke two-valve engine with a bowl in the piston is considered for the analysis. The detail engine specifications are given in Table 1. The engine geometry is modeled using PTC CREO 3.0 package.

3. The CFD analysis

In this study, the CFD analysis is carried out using CONVERGE, a commercial CFD package. The CONVERGE uses a fully automatic structured grid generation technique for

Table 1 The engine specifications.

Bore	87.5 mm
Stroke	110 mm
Connecting rod length	232 mm
Compression ratio	10:1
Rated engine speed	2000 rev/min
Maximum intake valve lift	7.9 mm
Nozzle hole diameter	0.15 mm
Number of injector holes	6
Fuel injector orientation	56°
Fuel injector hole length	1.1 mm
Fuel spray cone angle	15°
IVO: 4.5 CAD bTDC	EVO: 35 CAD bBDC
IVC: 35 CAD aBDC	EVC: 4.5 CAD aTDC

meshing a geometry during run time [14]. The grid independence study is carried out for the engine under consideration, as per Krishna et al. [15]. The flow turbulence is analyzed using the renormalized group (RNG) k - ϵ model [16,17]. The finite volume-based implicit discretization procedure is used to solve the discretized Navier–Stokes’ equations on a Cartesian grid. The in-cylinder flow is modeled by solving mass, momentum and energy conservation equations along with the equations for species, turbulent kinetic energy (TKE) and turbulent dissipation rate at each cell and at each time step. The “pressure implicit for splitting of operator” (PISO) algorithm is used to solve the pressure-velocity coupling. The spray analysis is carried out using kh-rt spray model [18]. The engine combustion is modeled using SAGE detailed chemistry solver proposed by Senecal et al. [19].

The base grid size used in this study is 4 mm. In the cylinder and valve regions, the grid is embedded permanently to a level of 2 which changes the grid in these regions to 1 mm. Further, the grid is refined in the regions of fuel spray and around the spark discharge point during the corresponding events to a size that changes between 0.125 and 0.25 mm. The adaptive mesh refinement is also used to capture the gradients of velocity, temperature and chemical species. The cylinder, intake and exhaust flow regions are initialized with atmospheric conditions.

4. Validation of CFD models

4.1. Spray model

In this study, the fuel spray atomization is analyzed using the kh-rt model [18]. Li et al. [20] captured images of the fuel spray pattern in a constant-volume chamber using a high speed CCD camera. Experimental conditions used by Li et al. [20] are given in Table 2. In this study, the CFD analysis is carried out at the similar conditions as that of Li et al. [20], in order to compare the predicted fuel spray penetration length with that of the experimental results of Li et al. [20].

Fig. 1 shows the comparison of fuel spray penetration lengths as predicted by kh-rt model in the present study and those of the Li et al. [20]. From Fig. 1, it is seen that, the fuel spray penetration length is under predicted by the kh-rt model at the beginning of the fuel injection. However, as the fuel spray evolves further, the kh-rt model is able to predict the fuel spray penetration length with a minimum deviation of less than 1% at 1.8 ms. After a time period of 2 ms, the fuel spray penetration length is over predicted by about 5%. The maximum deviation in the fuel spray penetration length between the experimental and the CFD analyses is about 10%. The overall performance of kh-rt model to predict the fuel spray structure and the tip penetration is reasonably good and hence it is used, in this study, for the further CFD analysis with a confidence.

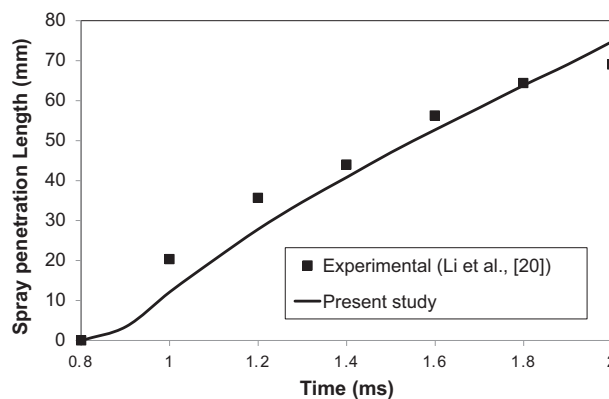


Figure 1 Comparison of spray penetration length in the constant-volume chamber.

In the range of fuel pressures considered, there is no change in the kh-rt model constants. However, the fuel injection duration varies depending on the engine speed and fuel injection pressure. A summary of fuel injection duration for various cases is given in Table 3.

4.2. Combustion and emission modelling

The turbulence and combustion models used in the present study are validated by using the experimental data of Li [21]. He conducted the experimental and numerical investigations on a four-valve single-cylinder DISI engine. The engine specifications used by him are given in Table 4 [20,21].

In this study, the present CFD results of variation of in-cylinder pressure with crank angle are compared with those of the experimental results of Li [21] during the following: (i) motoring conditions at 800 rev/min, and (ii) firing conditions at 1500 rev/min as shown in Fig. 2. From Fig. 2, it can be observed that, there is a good agreement among the present CFD and experimental results of Li [21], with a maximum deviation of about 2%. In addition, the variation of TR with crank angle from the present study is compared with that of Li et al. [20] as shown in Fig. 3. From Fig. 3, it is also seen that, the predicted TR from the present study is in reasonably good agreement with that of Li et al. [20], with a maximum deviation of about 3%.

5. Results and discussion

In this study, the CFD analysis is carried out on a four-stroke two-valve air-cooled GDI engine, in order to understand the effect of various engine parameters on the performance and emission characteristics of the engine. Fig. 4 shows the cases considered in the present study. The input parameters are the engine speed, compression ratio and fuel injection pressure,

Table 2 Experimental conditions used for constant-volume chamber test [20].

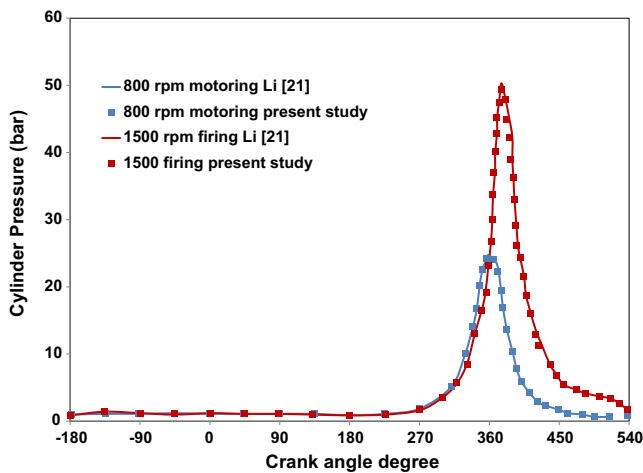
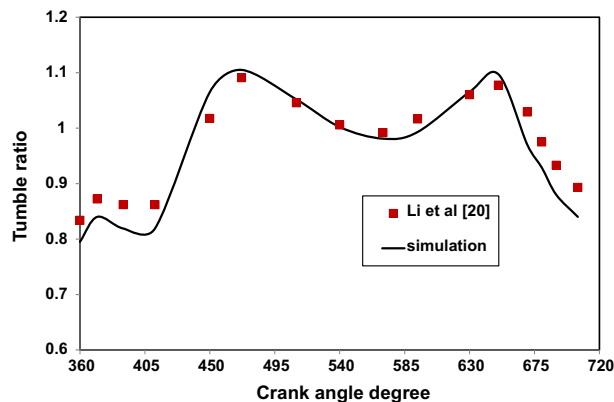
Chamber size	Fuel injection pressure	Chamber pressure	Chamber temperature	Injection duration (ms)
40 mm diameter 200 mm depth	100 bar	1 bar	20 °C	2

Table 3 Fuel injection duration for various cases.

Engine speed (rev/min)	Fuel injection pressure (bar)	Fuel injection duration (CAD)
2000	200	62.0
2000	300	50.5
2000	400	43.8
3000	200	93.0
4000	300	123.0

Table 4 The engine specifications [20,21].

Bore	89.0 mm
Stroke	90.3 mm
Connecting rod length	154 mm
Compression ratio	11.3:1
IVO	16 CAD before TDC
EVC	37 CAD after TDC

**Figure 2** Comparison of in-cylinder pressure under motoring and firing conditions.**Figure 3** Comparison of TR under firing conditions.

whereas the parameters considered for the comparison are TKE, TR, peak pressure, IMEP, NO_x and HC emissions.

In all the following figures presented, 360 CAD refers to the suction TDC and 720 CAD refers to the combustion TDC.

For all the cases considered, the equivalence ratio is maintained at 0.75. The spark timing is kept at 20 CAD before TDC. The SOI is maintained at 90 CAD before TDC. The end of fuel injection is based on the equivalence ratio and fuel injection pressure, for each case.

5.1. Effect of engine parameters on the TKE

5.1.1. Effect of fuel injection pressure on the TKE

Fig. 5 shows the variation of TKE with crank angle for the three fuel injection pressures of 200, 300 and 400 bar. From Fig. 5, in all the cases, it is observed that, the TKE varies with crank angle after the fuel injection event. This is because of the transfer of momentum from the injected fuel to the surrounding air. From Fig. 5, it is also observed that, the rise in TKE is maximum when the fuel injection pressure is 400 bar. At higher fuel injection pressures, the shear deformation of air molecules at the periphery of fuel jet is higher which results in higher fluctuating components of velocity at this region. Therefore, the TKE increases at higher fuel injection pressures. Also, the peak TKE after the fuel injection is about 21 and 40.2% higher with the fuel injection pressures of 300 and 400 bar, compared to that of the 200 bar.

5.1.2. Effect of compression ratio on the TKE

Fig. 6 shows the variation of TKE with crank angle for three CRs of 10, 11 and 12. From Fig. 6, it is observed that, the peak TKE is higher at lower CR. However, the TKE at the time of spark is more important than the peak TKE, as it decides the flame propagation rate. From Fig. 6, it is also seen that, at the time of spark (at 700 CAD), the TKE is higher for the lower CR. As the CR increases from 10 to 11 and 12, the TKEs at the time of spark decrease by about 39 and 70% respectively. This is because, at higher CRs, the compact cylinder volume along with reduced molecular space restricts air motion inside the cylinder which results in reduction in mean and fluctuating components of velocity. Also, it is found that, at all the CRs, the TKE increases because of fuel injection as shown in Fig. 6. A similar trend is also observed by Mural Krishna et al. [22,23].

5.1.3. Effect of engine speed on the TKE

Fig. 7 shows the variation of TKE with crank angle at three engine speeds of 2000, 3000 and 4000 rev/min. From Fig. 7, it can be seen that, the TKE increases with engine speed. The velocity of air entering the engine cylinder during suction stroke is higher at higher engine speeds which results in the higher peak TKE. However, the flame propagation is mainly affected by the level of TKE at the time of spark. From Fig. 7, it is also observed that, the TKE level at the time of spark (700 CAD) is lower for lower engine speeds. When the engine speed increases from 2000 to 3000 and 4000 rev/min, the TKE increases by about 111 and 338% respectively. The second peak of the TKE is observed after the fuel injection, which has a significant effect. In this case, the TKE after the fuel injection is higher for higher engine speeds and it is lower at lower engine speeds even though the fuel injection pressure is constant. This is because, at higher engine speed, the TKE is already at a higher value before the fuel injection. After the fuel injection, the TKE is further enhanced because of the momentum transfer between the fuel jet and the surrounding

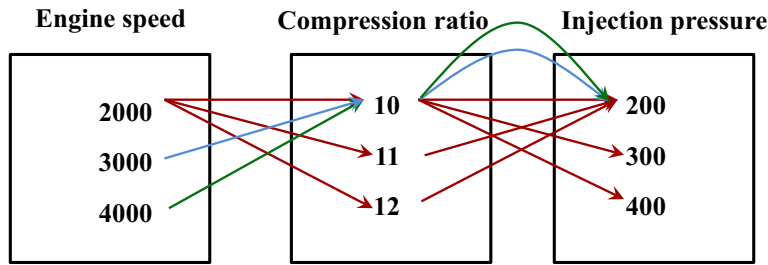


Figure 4 Cases considered for the CFD analysis.

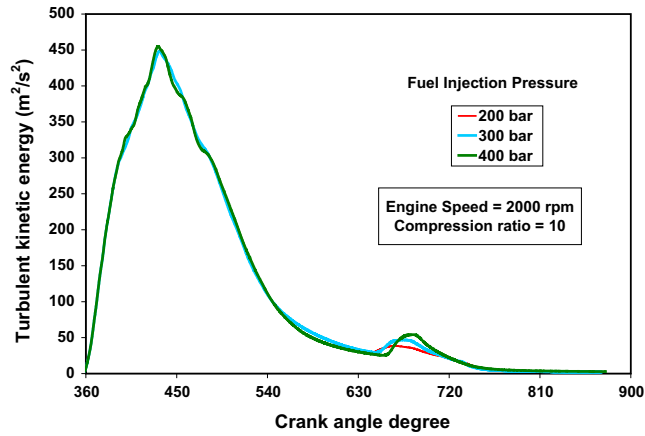


Figure 5 Variation of TKE with crank angle for various fuel injection pressures.

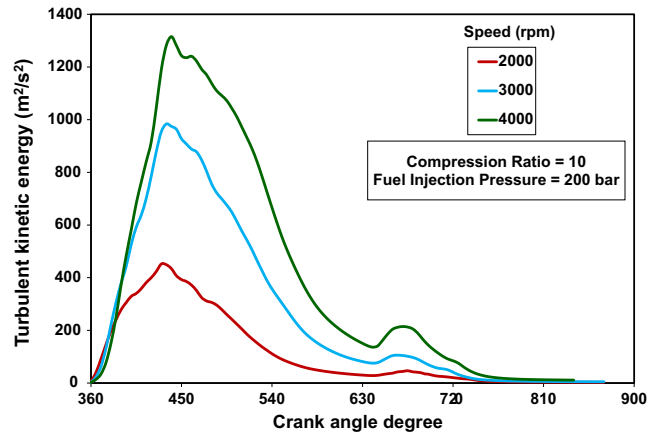


Figure 7 Variation of TKE with crank angle for various engine speeds.

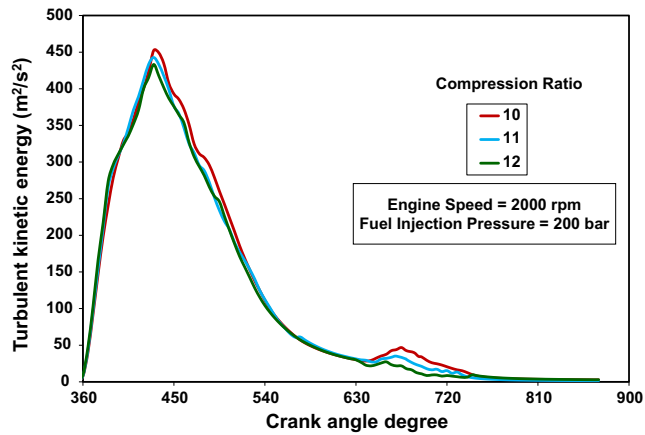


Figure 6 Variation of TKE with crank angle for various compression ratios.

air. However, at the lower engine speed, the TKE before the fuel injection is low. Hence, the rise in the TKE is lower after the fuel injection when the fuel injection pressure is maintained constant.

5.2. Effect of engine parameters on the TR

5.2.1. Effect of fuel injection pressure on the TR

The TR governs the mixture formation and availability of combustible air-fuel mixture near the spark plug. Hence, its

value from the beginning of fuel injection till the time of spark discharge directly affects the performance and emission characteristics of the engine. In the present study, the TR is evaluated based on Eq. (1) as

$$TR = \frac{\omega_i}{\omega_{crank\ shaft}} \tag{1}$$

where ω_i is the angular speed of flow in i direction and $\omega_{crank\ shaft}$ is the angular speed of crank shaft [16,23].

Fig. 8 shows the variation TR of in-cylinder flow with crank angle for three fuel injection pressures viz., 200, 300 and 400 bar. The TR represents the strength of bulk fluid motion in the engine cylinder. The high pressure fuel injection certainly disturbs the bulk motion of the in-cylinder flow. However, from Fig. 8, it is observed that, the effect of fuel injection pressure on bulk motion of air is negligible. This is because of symmetrical positioning of fuel injector holes about the axis of the injector. This makes the fuel spray to spread in either side of the fuel injector in a symmetrical manner which nullifies its effect by the opposing in-cylinder flows. Therefore, the fuel injection pressure does not have much influence on the TR.

5.2.2. Effect of compression ratio on TR

Fig. 9 shows the variation of TR with crank angle at three compression ratios viz., 10, 11 and 12. From Fig. 9, it is found that, the TR does not vary much till 540 CAD (BDC). From Fig. 9, it is also observed that, the magnitude of TR after 540 CAD, reduces as the CR increases. At higher CRs, the combustion chamber volume reduces, which restricts in-

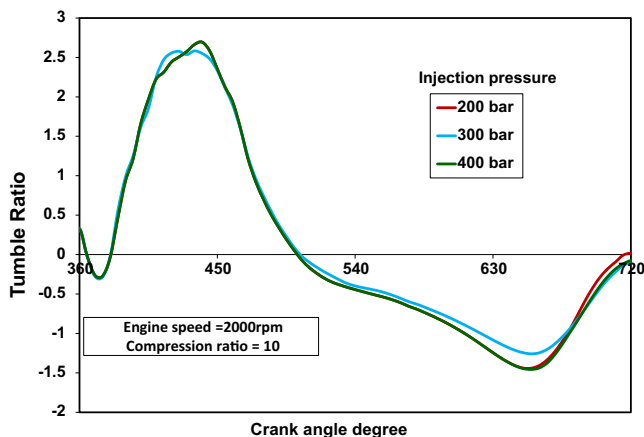


Figure 8 Variation of TR with crank angle for various fuel injection pressures.

cylinder fluid motion and thus TR reduces. At the beginning of the fuel injection (at 630 CAD), when the CR increases from 10 to 11 and 12, the TR decreases by about 16.7% and 50% respectively. Similarly, at the time of spark (at 700 CAD), when the CR increases from 10 to 11 and 12, the TR decreases by about 24.5% and 37.3% respectively. The trends of variations of TRs as observed, in this study, are similar to those obtained by Murali Krishna et al. [23,22].

5.2.3. Effect of engine speed on TR

Fig. 10 shows the variation of TR with crank angles for three engine speeds viz., 2000, 3000 and 4000 rev/min. From Fig. 10, it can be observed that, the TR is higher at higher engine speeds during the fuel injection phase. The rise in the TR due to increase in the engine speed is because of higher piston velocity at higher engine speeds which helps tumble motion. The TR, at the start of injection (at 630 CAD), is more by about 9 and 22% at 3000 and 4000 rev/min, respectively than that of at 2000 rev/min. However, the change in the TR is insignificant at the time of spark (at 700 CAD), because of the restriction of air motion as the piston approaches TDC.

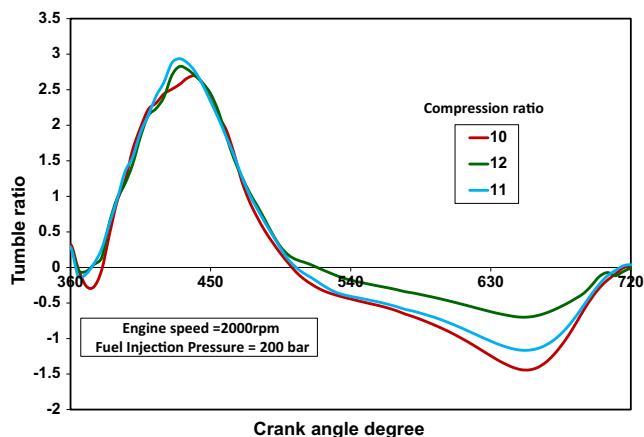


Figure 9 Variation of TR with crank angle for various compression ratios.

5.3. Effect of engine parameters on the peak in-cylinder pressure

5.3.1. Effect of fuel injection pressure on the peak in-cylinder pressure

The fuel injection pressure along with TR plays an important role in the mixture formation which in turn affects the peak in-cylinder pressure of the engine [26]. Fig. 11 shows the variation of in-cylinder pressure with crank angles for the three fuel injection pressures viz., 200, 300 and 400 bar. From Fig. 11, it is observed that, at the fuel injection pressures of 200 and 300 bar, the peak in-cylinder pressures are about 77 and 82 bar respectively. However, when the fuel injection pressure is about 400 bar, the combustion does not take place at all. Fig. 12 shows the variation of equivalence ratio in the combustion chamber at the time of spark, for the various fuel injection pressures. From Fig. 12, it is seen that, at the fuel injection pressure of 400 bar, the ignitable air-fuel mixture doesn't exist at the location of the spark plug.

Thereby, there won't be any pressure rise due to combustion, and thus in-cylinder pressure curve simply follows the motoring pressure curve. Further, from Fig. 11, it is observed that, the occurrence of the peak pressure marginally shifts toward the TDC at the fuel injection pressure of 300 bar, which is mainly because of the reduced ignition delay due to better atomization of the fuel. Also, we found that, the level of the peak pressure rises by about 5% when the fuel injection pressure increases from 200 to 300 bar.

5.3.2. Effect of compression ratio on the peak in-cylinder pressure

Fig. 13 shows the variation of in-cylinder pressure with crank angles for three compression ratios viz., 10, 11 and 12.

From Fig. 13, it is observed that, the peak in-cylinder pressure increases with increase in the CR. At higher CRs, the in-cylinder pressure at the end of compression stroke is higher which results in higher peak in-cylinder pressure after the combustion. From Fig. 13, it is also observed that, the occurrence of the peak in-cylinder pressure shifts marginally toward the TDC, when the CR increases. This is because of better mixing of air and fuel which happens at higher CRs owing to less in-cylinder volume which results in lower ignition delay. It is also found that, the increase in CR from 10 to 11 and 12, results in

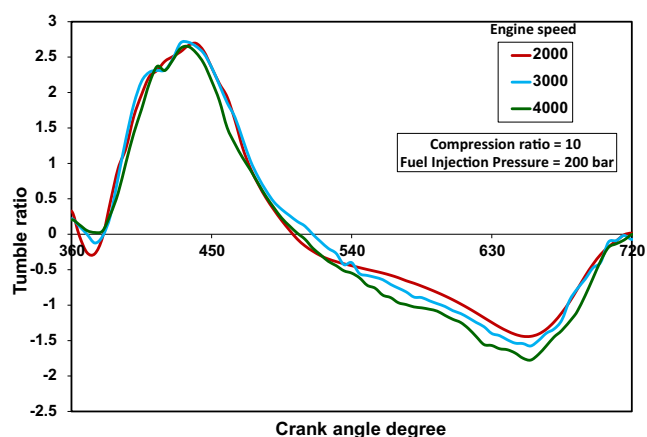


Figure 10 Variation of TR with crank angle for various engine speeds.

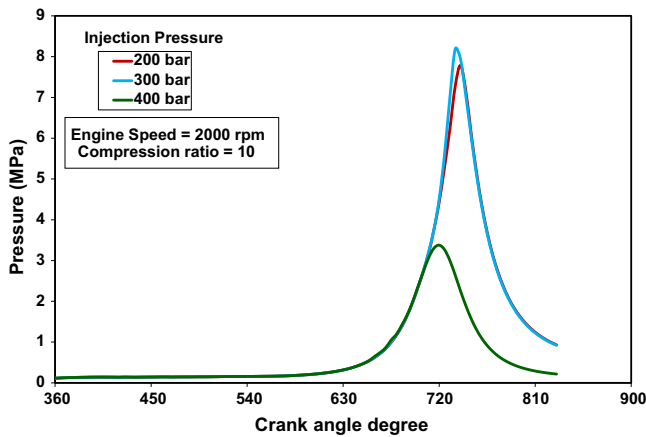


Figure 11 Variation of in-cylinder pressure with crank angle for various fuel injection pressures.

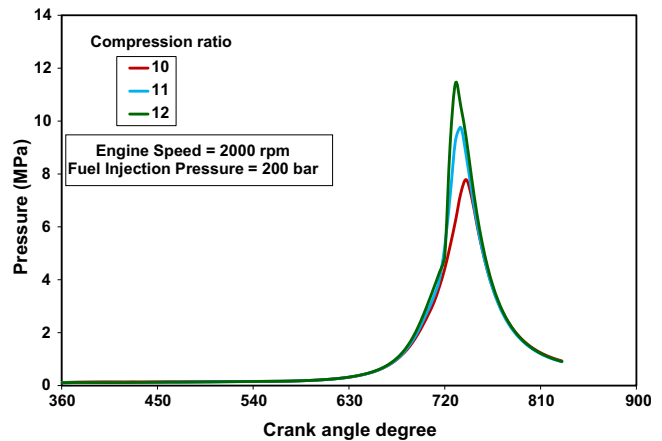


Figure 13 Variation of in-cylinder pressure with crank angle for various compression ratios.

the rise of the peak in-cylinder pressure by about 22.8 and 42% respectively. High in-cylinder peak pressure like what is observed in this case was also observed by Semin et al., [24], in their work, with an engine of similar capacity.

5.3.3. Effect of engine speed on the peak in-cylinder pressure

Fig. 14 shows the variation of in-cylinder pressure with crank angles at three engine speeds viz., 2000, 3000 and 4000 rev/min. From Fig. 14, it is observed that, the peak in-cylinder pressure rises when the engine speed increases from 2000 to 3000 rev/min. However, when the engine speed increases to 4000 rev/min, the rise in the peak in-cylinder pressure is not observed. This is because, at 4000 rev/min, the heat transfer rate from cylinder gases to cylinder wall will be higher, which results in slow combustion [25–28]. This may also be because of the wall guided fuel injection mode of operation of the engine, which is very sensitive to the operating conditions. Further, from Fig. 15, it is seen that, at the engine speed of 4000 rev/min, the rate of heat release is lesser compared to

those of the other two engine speeds. This can also be seen from the growth of flame front at various crank angles after the ignition as shown in Fig. 16. From Fig. 16, it is seen that, the flame propagation rate is slower at 4000 rev/min. It is also found that, the occurrence of the peak pressure advances, when the engine speed rises from 2000 to 3000 rev/min. This is because of higher TR at the engine speed of 3000 rev/min, which helps better mixing of air and fuel, thereby reducing the ignition delay.

5.4. Effect of engine parameters on the IMEP

5.4.1. Effect of fuel injection pressure on the IMEP

Fig. 17 shows the variation of IMEP for various fuel injection pressures viz., 200, 300 and 400 bar. In this study, the IMEP is calculated based on the indicated work during the closed part of the cycle (35 CAD after BDC to 4.5 CAD after TDC). From Fig. 17, it is found that, the IMEP is almost the same for the

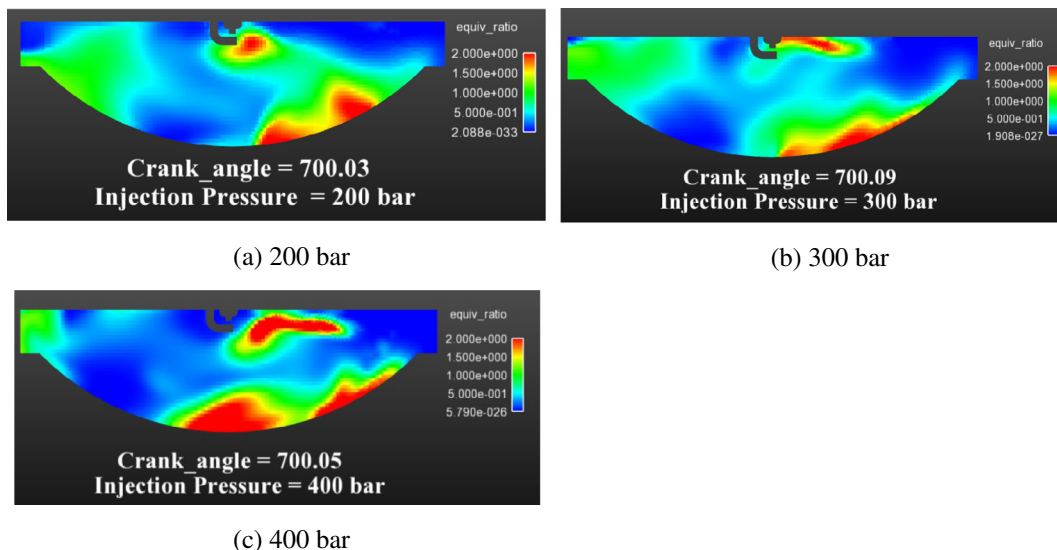


Figure 12 Equivalence ratio distribution in the combustion chamber at the time of spark for various fuel injection pressures.

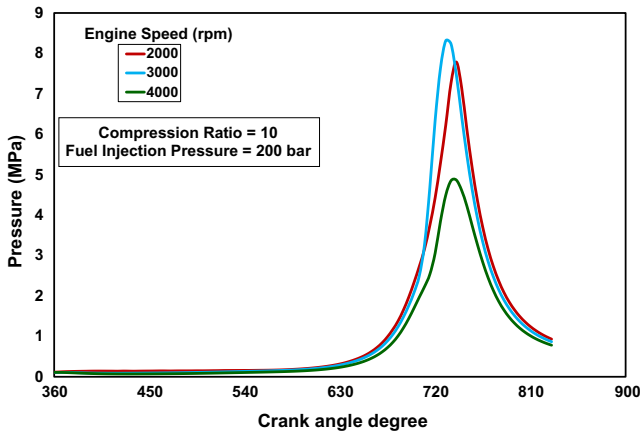


Figure 14 Variation of in-cylinder pressure with crank angles at various engine speeds.

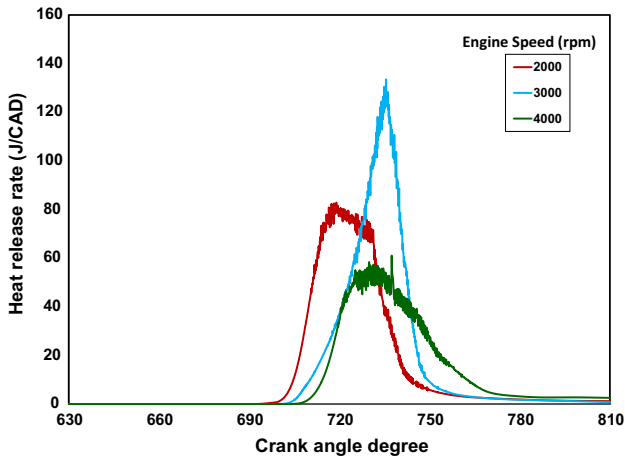


Figure 15 Variation of heat release rate with crank angles at various engine speeds.

fuel injection pressures of 200 and 300 bar. However, at 400 bar, because of misfiring, the IMEP is zero.

5.4.2. *Effect of compression ratio on the IMEP*

Fig. 18 shows the variation of IMEP for various CRs viz., 10, 11 and 12. As the peak in-cylinder pressure rises with CR, the IMEP also increases. From Fig. 18, it is observed that, the IMEP increases by about 2.5% and 4%, when the CR increases from 10 to 11 and 12 respectively.

5.4.3. *Effect of engine speed on the IMEP*

Fig. 19 shows the variation of IMEP for various engine speeds viz., 2000, 3000 and 4000 rev/min. It is well known that, the IMEP is independent of engine speed. From Fig. 19, it is found that, the IMEP remains constant when the engine speed changes from 2000 to 3000 rev/min.

However, the IMEP reduces significantly, when the engine speed is 4000 rev/min, because of slow combustion as explained in Section 5.3.3.

5.5. *Effect of engine parameters on the NOx formation and emissions*

5.5.1. *Effect of fuel injection pressure on the NOx formation and emissions*

Fig. 20 shows the variation of NOx formation with crank angles at various fuel injection pressures viz., 200, 300 and 400 bar. From Fig. 20, it is observed that, the NOx formation increases steadily from the time of spark until for about 20 CAD after TDC. This is because of increase in the gas temperature beyond 1700 K during combustion. Afterward, their formation is frozen and concentration remains constant up to the EVO. This is because, the gas temperature decreases during the expansion stroke, which inhibits the NOx formation.

From Fig. 20, it is also observed that, the NOx levels are higher at higher fuel injection pressures. This is because of

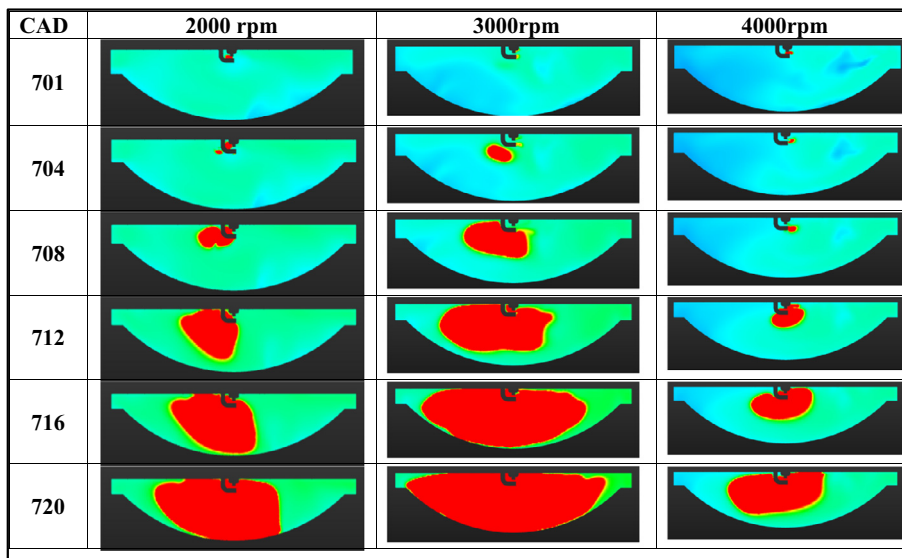


Figure 16 Comparison of flame propagation with crank angles at various engine speeds.



Figure 17 Variation of IMEP with various fuel injection pressures.

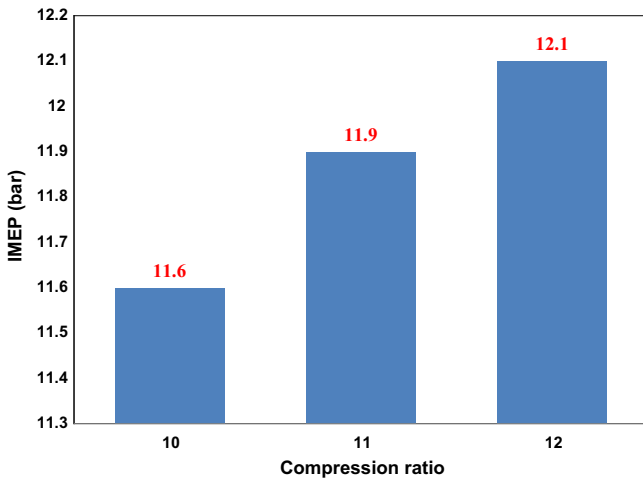


Figure 18 Variation of IMEP with various compression ratios.

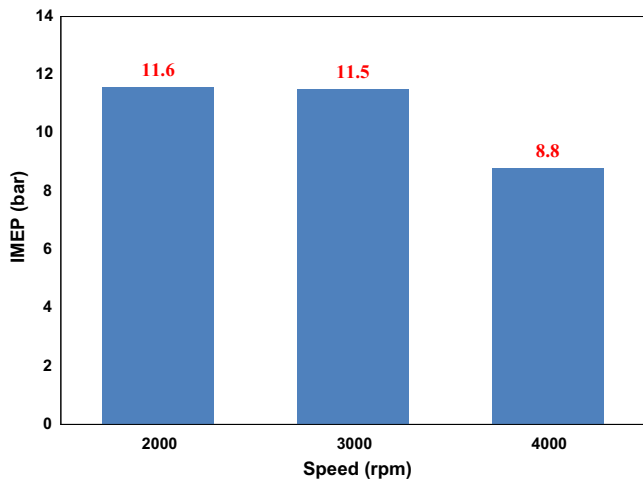


Figure 19 Variation of IMEP with various engine speeds.

higher in-cylinder temperature during combustion, at higher fuel injection pressures. However, because of misfiring, no NOx formation is observed at the fuel injection pressure of 400 bar. From Fig. 20, it is also found that, at the fuel injection pressure of 200 bar, the NOx emissions at the EVO, are about 3292 PPM, whereas for 300 bar, they are about 3700 PPM. It is also found that, the NOx emissions from the engine are about 12% higher when the fuel injection pressure increases from 200 to 300 bar.

5.5.2. Effect of compression ratio on NOx formation and emissions

Fig. 21 shows the variation of NOx formation with crank angles for various CRs viz., 10, 11 and 12, from the time of spark to the EVO. From Fig. 21, it is seen that, the NOx formation is higher at higher CR. This is because, the peak in-cylinder temperature increases with increase in CR, thus giving rise to higher NOx levels. It is found that, the NOx emissions at the EVO, at the CR of 10, are about 3292 PPM, whereas they are about 3600 and 4980 PPM respectively, when the CRs are 11 and 12. From Fig. 21, it is observed that, the

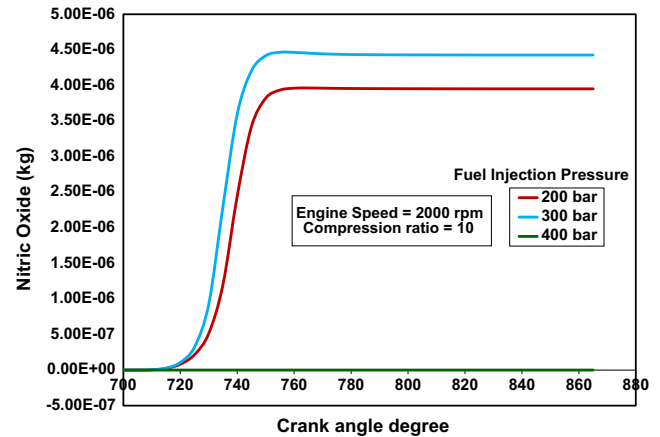


Figure 20 Variation of NOx formation with crank angles for various fuel injection pressures.

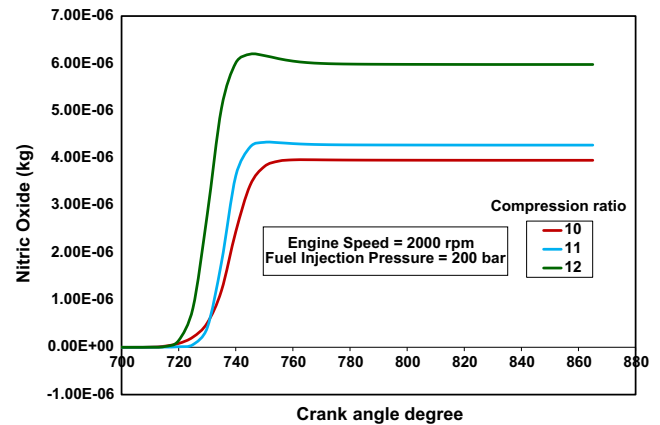


Figure 21 Variation of NOx formation with crank angles for various compression ratios.

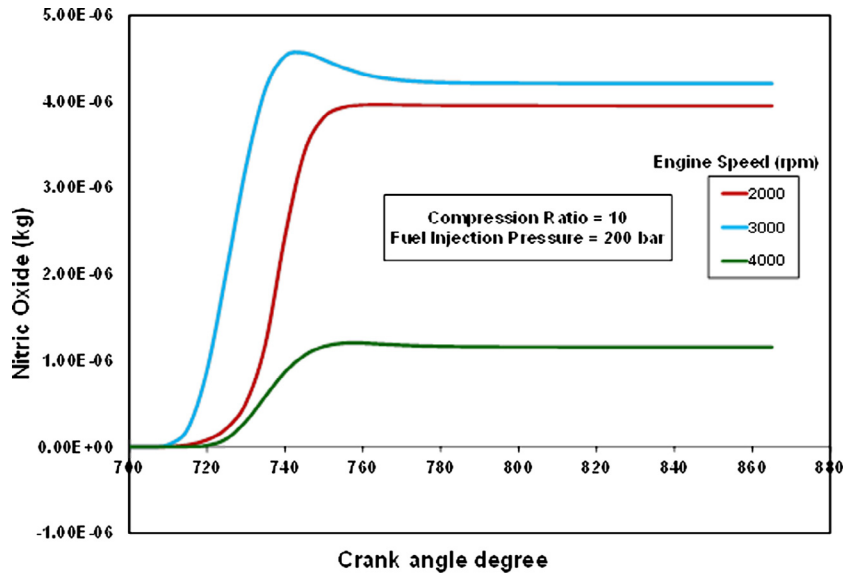


Figure 22 Variation of NOx formation with crank angles for various engine speeds.

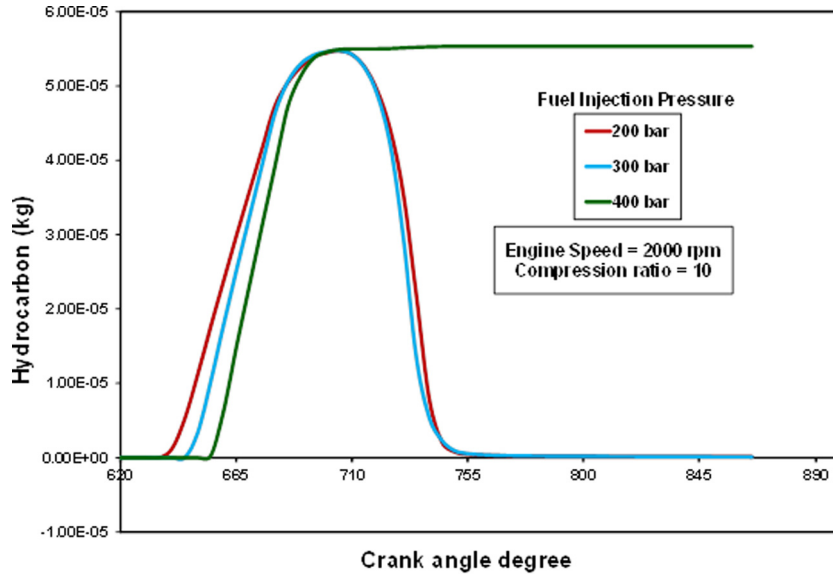


Figure 23 Variation of HC concentration with crank angles for various fuel injection pressures.

NOx emissions are higher by about 8 and 51%, when the CR increases from 10 to 11 and 12 respectively.

5.5.3. Effect of engine speed on the NOx formation and emissions

Fig. 22 shows the variation of in-cylinder NOx formation with crank angles at various engine speeds viz., 2000, 3000 and 4000 rev/min. From Fig. 22, it is found that, the NOx formation increases marginally with increase in the engine speed. This is because of rise in peak in-cylinder pressure, with the increase in the engine speed, which results in the increase in peak in-cylinder temperature. However, from Fig. 22, it is also observed that, the NOx formation levels are lower at the engine speed of 4000 rev/min, which is because of slower com-

bustion as explained in Section 5.3.3. From Fig. 22, it is observed that, the levels of NOx emissions, for 2000, 3000 and 4000 rev/min, are about 3292, 3500 and 960 PPM respectively. At the engine speed of 3000 rev/min, the NOx emissions are about 6.5% higher compared to those of 2000 rev/min.

5.6. Effect of engine parameters on the HC formation and emissions

5.6.1. Effect of fuel injection pressure on the HC formation and emissions

Fig. 23 shows the variation of HC formation with crank angles at various fuel injection pressures viz., 200, 300 and 400 bar. From Fig. 23, it is observed that, for the fuel injection pres-

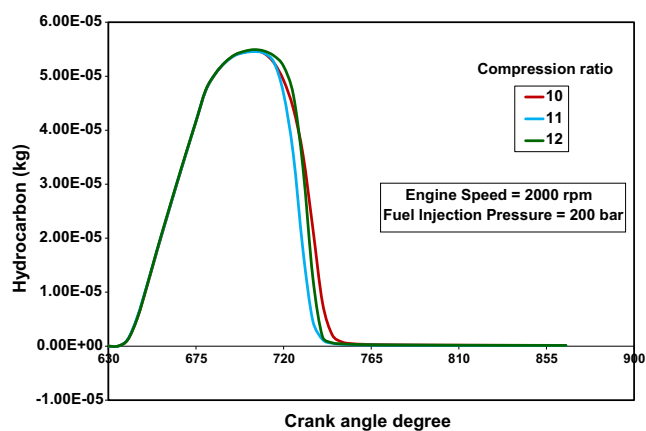


Figure 24 Variation of HC concentration with crank angles for various compression ratios.

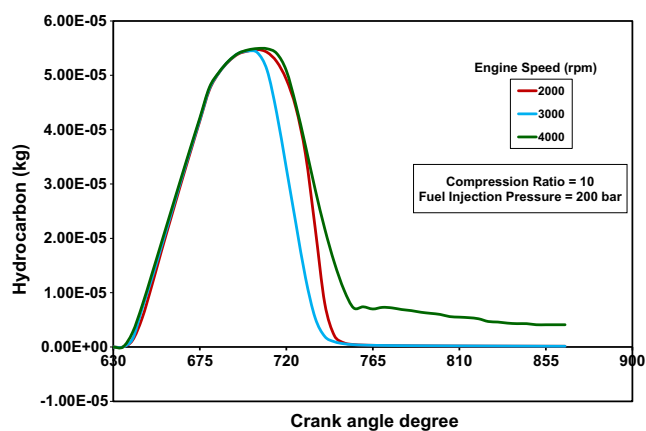


Figure 25 Variation of HC concentration with crank angles for various engine speeds.

tures of both 200 and 300 bar, the HC emissions are very low after 750 CAD. However, at the fuel injection pressure of 400 bar, because of misfiring, the HC emissions shoot up. In fact, in this case, combustion does not take place at all. Therefore, the entire injected fuel remains as it is, in the cylinder and exhausted. For both the fuel injection pressures of 200 and 300 bar, the HC emissions, at the EVO, are lesser than 100 PPM.

5.6.2. Effect of compression ratio on the HC formation and emissions

Fig. 24 shows the HC concentration with crank angles for three CRs of 10, 11 and 12. From Fig. 24, it is observed that, the HC concentration is closer to zero, in all the cases, because of the complete combustion of the injected fuel.

5.6.3. Effect of engine speed on the HC formation and emissions

Fig. 25 shows the variation of HC concentration with crank angles for various engine speeds viz., 2000, 3000 and 4000 rpm. From Fig. 25, it is observed that, the HC concentrations are about 100 PPM at the engine speeds of 2000 and 3000 rev/min. However, at the engine speed of 4000 rev/min, the HC emissions are high, because of reasons as explained

earlier. At the engine speed of 4000 rev/min, the HC emissions, at the EVO, are about 3500 PPM.

6. Conclusions

The present paper discusses the effect of various engine parameters on the performance and emission characteristics of a two-valve four-stroke GDI engine by the CFD analysis. The computational models used in the CFD analysis have been thoroughly validated against the experimental data available in the literature. From the results, the following conclusions are drawn:

- When the fuel injection pressure increases from 200 to 300 and 400 bar:
 - The TKE increases by about 21 and 40.2% after the fuel injection.
 - The TR is not much affected by the fuel injection pressure.
- It is also found that, the lower fuel injection pressures (200 and 300 bar) are better in order to get an ignitable mixture at the spark plug location, at the time of spark. Higher fuel injection pressure (400 bar) results in misfiring of the engine.
- When the CR increases from 10 to 11 and 12:
 - At the time of spark, the TKE decreases by about 39 and 70% respectively. The TR decreases by about 16.7 and 50% respectively.
 - The IMEP increases by about 2.5 and 4% respectively.
 - The NOx emissions increase by about 8 and 51% respectively.
 - The HC emissions are very low, in all the cases.
- When the engine speed increases from 2000 to 3000 and 4000 rev/min:
 - The TKE increases by about 111 and 331% respectively.
 - The TR increases by about 9 and 21% respectively.
 - The NOx emissions increase by about 6.5 and -71% respectively.
 - The HC emissions are nearly zero for 2000 and 3000 rev/min, whereas they are about 3500 PPM at 4000 rev/min, respectively.

References

- [1] L. Spiegel, U. Spicher, Mixture formation and combustion in a spark ignition engine with direct fuel injection, SAE paper no. 920521, 1992.
- [2] M.C. Drake, T.D. Fansler, A.M. Lippert, Stratified-charge combustion: modeling and imaging of a spray-guided direct-injection spark-ignition engine, *Proc. Combust. Inst.* 30 (2005) 2683–2691.
- [3] R. Banerjee, S. Kumar, Numerical investigation of stratified air/fuel preparation in a GDI engine, *Appl. Therm. Eng.* 104 (2016) 414–428.
- [4] F.Q. Zhao, M.C. Lai, D.L. Harrington, A review of mixture preparation and combustion control strategies for spark-ignited direct-injection gasoline engines, SAE paper no. 970627, 1997.
- [5] A.S. Krishna, J.M. Mallikarjuna, Davinder Kumar, Effect of engine parameters on in-cylinder flows in a two-stroke gasoline direct injection engine, *Appl. Energy* 176 (2016) 282–294.

- [6] J. Suresh Kumar, V. Ganesan, J.M. Mallikarjuna, G. Srinivasan, Effect of piston crown shape on in-cylinder flow characteristics in a direct injection engine – a CFD study, SAE paper no. 2013-01-2797, 2013.
- [7] H. Oh, C. Bae, Effects of the injection timing on spray and combustion characteristics in a spray-guided DISI engine under lean-stratified operation, *Fuel* 107 (2013) 225–235.
- [8] H. Baecker, A. Kaufmann, M. Tichy, Experimental and simulative investigation on stratification potential of spray-guided GDI combustion systems, SAE paper no. 2007-01-1407, 2007.
- [9] C. Stan, A. Stanciu, R. Troeger, L. Martorano, C. Tarantino, M. Antonelli, R. Lensi, Influence of mixture formation on injection and combustion characteristics in a compact GDI engine, SAE paper no. 2002-01-0997, 2002.
- [10] S. Lee, S. Park, Experimental study on spray break-up and atomization processes from GDI injector using high injection pressure up to 30 MPa, *Int. J. Heat Fluid Flow* 45 (2014) 14–22.
- [11] P. Sementa, B.M. Vaglieco, F. Catapano, Thermodynamic and optical characterizations of a high performance GDI engine operating in homogeneous and stratified charge mixture conditions fueled with gasoline and bio-ethanol, *Fuel* 96 (2012) 204–219.
- [12] Z. Zheng, C. Liu, X. Tian, X. Zhang, Numerical study of the effect of piston top contour on GDI engine performance under catalyst heating mode, *Fuel* 157 (2015) 64–72.
- [13] M. Costa, L. Marchitto, S.S. Merola, U. Sorge, Study of mixture formation and early flame development in a research GDI (gasoline direct injection) engine through numerical simulation and UV-digital imaging, *Energy* 77 (2014) 88–96.
- [14] CONVERGE v2.2.0, Theory Manual, Convergent Science Inc, 2015.
- [15] A.S. Krishna, J.M. Mallikarjuna, Effect of fuel injector location on the equivalence ratio near the spark plug in a GDI engine – a CFD analysis, in: 24th National Conference on Internal Combustion Engines and Combustion, Oct 30th –Nov 1st, Dehradun India, 2015.
- [16] A.S. Krishna, J.M. Mallikarjuna, K. Davinder, Y.R. Babu, In-cylinder flow analysis in a two-stroke engine – a comparison of different turbulence models using CFD, SAE paper no. 2013-01-1085, 2013.
- [17] V. Yakhot, S.A. Orszag, S. Thangam, T.B. Gatski, C.G. Speziale, Development of turbulence models for shear flows by a double expansion technique, *Phys. Fluids A4* (7) (1994).
- [18] Y. Imaoka, K. Shouji, T. Inoue, T. Noda, A study of a multistage injection mechanism for improving the combustion of direct-injection gasoline engines, SAE paper no. 2015-01-0883, 2015.
- [19] P.K. Senecal, E. Pomraning, K.J. Richards, Multi-dimensional modeling of direct injection diesel spray liquid length and flame lift-off length using CFD and parallel detailed chemistry, SAE paper no. 2003-01-1043, 2003.
- [20] H. Li, C. Li, X. Ma, P. Tu, H. Xu, S. Shuai, A. Ghafourian, Numerical study of DMF and gasoline spray and mixture preparation in a GDI engine, SAE paper no. 2013-01-1592, 2013.
- [21] H. Li, CFD modelling study of sprays and combustion of gasoline and DMF in direct injection gasoline engines Thesis, The University of Birmingham, 2013.
- [22] B. Murali Krishna, J.M. Mallikarjuna, Effect of compression ratio on in-cylinder tumble flows in an unfired internal combustion, in: ASV11-01-04, The 11th Asian Symposium on Visualization, Niigata, Japan, June 5–9, 2011, 2011, pp. 5–9.
- [23] B. Muralikrishna, Studies in in-cylinder tumble flows in an unfired internal combustion engine using particle image velocimetry Thesis, IIT Madras, 2010.
- [24] A.R. Ismail, T.F. Nugroho, Experimental and computational of engine cylinder pressure investigation on the port injection dedicated CNG engine development, *J. Appl. Sci.* 10 (2010) 107–115.
- [25] S.R. Turns, *An Introduction to Combustion*, McGraw-Hill Inc, 1996.
- [26] J.B. Heywood, *Internal Combustion engine Fundamentals*, McGraw-Hill Inc, 1988.
- [27] M.M. Rahman, K.I. Hamada, M.M. Noor, K. Kadirgama, Influence of engine speed on heat transfer characteristics of port injection hydrogen fueled engine, in: Proceedings of the International Conference on Mechanical Engineering, (ICME2009) 26–28 December, Dhaka, Bangladesh, 2009.
- [28] A. Sanli, A.N. Ozsezen, I. Kilicaslan, M. Canakci, The influence of engine speed and load on the heat transfer between gases and in-cylinder walls at fired and motored conditions of an IDI diesel engine, *Appl. Therm. Eng.* 28 (2007) 1395–1404.